JOURNAL OF THERMOPHYSICS AND HEAT TRANSFER
Vol. 18, No. 2, April–June 2004

Nano- to Microscale Modeling by Cluster Potentials

J. K. Chen,* J. E. Beraun,* and R. Roybal*
U.S. Air Force Research Laboratory, Kirtland Air Force Base, New Mexico 87117
and
D. Y. Tzou†
University of Missouri—Columbia, Columbia, Missouri 65211

Cluster potentials have been derived in this work by integrating the Lennard–Jones (LJ) potential over specific physical domains defining the geometrical shapes of the molecular clusters. For microsystems involving loosely compacted cluster arrays, the asymptotic expressions of the cluster potential are derived and compared to the LJ potential. Capabilities in multiscale modeling are demonstrated by introducing physical boundaries as large clusters of a planar geometry. Numerical examples include pressure and heat-flux distributions in nanoarrays subjected to in-depth heating.

Nomenclature

A	=	constant in the general form of cluster potential
a, b	=	radii of spheres
C_1	=	constant in Lennard–Jones (LJ) potential
C_2	=	constant in LJ potential
c	=	central distance
d	=	distance
E	=	cluster potential
F	=	force
M	=	cluster mass
m	=	number densities
r	=	distance
U	=	molecular potential
x	=	radius of disks
α, β	=	constants in the general form of cluster potential
θ	=	polar angle or temperature
ρ	=	radial distance
Σ	=	pressure
ξ, η	=	attractive and repulsive exponents (cluster potential)

Subscripts and Superscripts

D-S	=	disk-to-sphere
i, j	=	molecule i and j
M-D	=	molecule-to-disk
M-S	=	molecule-to-sphere
M-W	=	molecule-to-wall
S-S	=	sphere-to-sphere
0	=	equilibrium
$*$	=	reference values
–	=	nondimensional quantities

Introduction

MOLECULAR-DYNAMICS (MD) simulation has been proven effective in modeling the various thermomechanical processes in microscale.[1–3] A two-volume symposium[4] was published in 1996, where the uses of MD simulations in solidification, microscale processing, as well as prediction of microscale thermophysical properties and microstructural surface modeling were collected. Recent review on the development of MD simulations can be found in Ref. 5, which covers a wider spectrum of MD simulations. In addition to the normal and modified Lennard–Jones (LJ) potentials, more sophisticated Stillinger and Weber[6] and Tersoff[7] potentials for silicon, the ab initio MD method describing electronic states by the Schrödinger wave equation to address the quantum-mechanical effects,[8,9] and the embedded-atom type potentials[10] were among the list. Gradient of the molecular potential gives rise to the force exerting on the molecules in support of their motion. Except for the equations of motion, which can either be Newton's law for describing classical behaviors or the Schrödinger wave equation to address the quantum-mechanical effects, the MD simulation does not require a constitutive relation known as a priori. Thermomechanical responses, including temperature and heat-flux vector in measuring energy-carrying capacities and stresses in evaluating load-bearing capacities, are calculated from the statistical averages that involve molecular positions, velocities, and energies in accordance with the virial theorem.[11,12] To describe the refined microstructures with sufficient details, the number of molecules involved in the computational cell ranges from hundreds (10^2) to 10^6, depending on the complexity of the targeted behaviors in the microsystem. As the number of molecules increases, to keep computational time manageable the cutoff radius is often introduced to eliminate the far-field forces. In the use of the LJ potential, for example, the cutoff radius is roughly taken as 2.6σ, with $(2^{1/6}\sigma)$ being the mechanical equilibrium position at which the intermolecular force is zero.

Complex microsystems can involve interactions between molecules and congregated molecular clusters forming various shapes. (Data available online at http://www.sc.doe.gov/production/bes/complexsystems.htm and http://www.sc.doe.gov/production/bes/nanoscale.html.) Evidenced by a nanotube with hexagonal clusters uniformly distributed on its circumference, it would require hundreds of thousands of molecules to model just one nanotube via classical MD simulations. Modeling a simple bundle of such nanotubes can easily exceed the limit of even the fastest supercomputers nowadays, making it necessary to develop more effective models to describe interactions involving multiscale species in the nanoscale assemblies. All functional nanomaterials would face the same challenge.[13] As hundreds of thousands of nanophase agglomerates are collected from a liquid-hydrogen-cooled tube, with tens and hundreds of molecules involved in each, interactions among such agglomerates would dominate the functionalities of the consolidated (sintered) nanophase materials rather than the individual molecules. Conventional MD simulation would be able to characterize such complex systems for assuring the targeted functionalities, but the numerical efforts will be immense.

Treating the interatomic LJ potential as the building block, we developed the cluster interaction potential.[14] Mathematically, the

Received 6 August 2003; revision received 6 November 2003; accepted for publication 7 November 2003.

*Laser Effects Research Branch, Directed Energy Directorate.
†James C. Dowell Professor, Department of Mechanical and Aerospace Engineering; TzouR@missouri.edu.

well-known LJ potential is used as the Green's function to derive the new potentials as numerous molecules congregate into various shapes. In special cases where the nanophase assemblies are loosely compacted, we emphasize variations of the attractive and repulsive exponents as the cluster shape varies. Full expression of the cluster potential is used in the cluster-dynamics (CD) simulation to treat nanophase assemblies in general, which now includes tightly compacted assemblies. One-dimensional heat flux (for the energy-carrying capacities) and stress (load-bearing capacities) are calculated and presented in the numerical example.

Cluster Potentials

A cluster (meso- or macroscopic body) is defined here as an assembly of like molecules (or atoms) that are compacted uniformly in a physical domain. Molecular clusters can exist naturally, such as the nanoparticles suspended in nanofluids.[15,16] The intermolecular bonds inside the nanoparticles are much stronger than those among the fluid molecules. Consequently, the solid-like nanoparticle could be modeled as a basic unit, or a cluster, when describing its interaction with the individual molecules of the fluid. Molecular clusters can also be formed as the individual molecules congregate, called agglomeration. The cluster concept can be introduced when agglomeration occurs, for saving the computational time caused by reduction of the interacting species in the computational domain, but additional criteria will be needed because such congregated molecules could also break. Breakup/recombination of molecular clusters falls into the category of dynamic clustering, which will be excluded in this work for the time being.

The size of a cluster can be as large as two to three orders of magnitude greater than a molecule (measured in angstroms). The pair potential between a molecule and a cluster is derived based on the assumption of additivity, the net interaction energy of the molecule, and the cluster is the sum of the interaction of the molecule with all of the molecules in the cluster. The same assumption is also applied to the pair potential between two clusters.

LJ potential is one of the most popular models used in the MD simulation because of its simple form and well-tabulated parameters for different materials,

$$U_{ij}(d_{ij}) = C_1 \big/ d_{ij}^{12} - C_2 \big/ d_{ij}^{6} \tag{1}$$

Typical values of C_1 and C_2 are of the order of 10^{-26} (J-nm^{12}) and $C_2 = 10^{-23}$ (J-nm^6), respectively.[1,2] The force between molecules is related to the potential function through the differential expression,

$$F_{ij} = -\frac{\partial U_{ij}}{\partial d_{ij}} = \frac{12C_1}{d_{ij}^{13}} - \frac{6C_2}{d_{ij}^{7}} \tag{2}$$

The repulsive force decays as d_{ij}^{-13}, and the attractive force decays as d_{ij}^{-7}. From Eq. (2) the equilibrium position is $d_0 = (2C_1/C_2)^{1/6}$, which corresponds to $F_{ij} = 0$. The corresponding potential at the location d_0 is $E_0 = C_2^2/(4C_1)$. The maximum attractive force is $F_s = -(126C_2^2/169C_1)/(26C_1/7C_2)^{1/6}$, occurring at the location $d_s = (26C_1/7C_2)^{1/6}$.

Spherical clusters are of interest in this work. Figure 1a shows the LJ potential U_{ij} between any pair of molecules i and j and the cluster potential $E(c)$ with c being the central distance between two spherical clusters. To determine the cluster potential, spheres A and B of radii a and b, respectively, are introduced in Fig. 1b. Molecules in each spherical cluster are assumed numerous, uniformly distributed throughout with the number densities of m_A (in sphere A) and m_B (in sphere B).

Molecule-to-Sphere Potential

Figure 2 illustrates the coordinate system employed for deriving the pair potential between a molecule P and sphere A. The molecule P can be considered a representative molecule in sphere B; the distance between the molecule P and center of sphere A is y'. Let (dr) be the thickness representative of a disk extracted from A and dA ($= \rho \mathrm{d}\rho \mathrm{d}\theta$) be an infinitesimal area. With $y = (\rho^2 + r^2)^{1/2}$ in place of

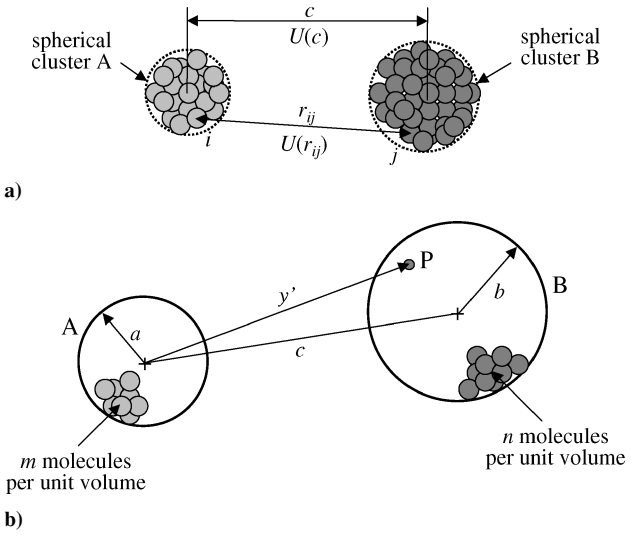

Fig. 1 Spherical clusters composed of uniformly compacted molecules: a) interaction potential $E(c)$ between clusters resulting from the LJ potential $U(r_{ij})$ between molecules i and j in the clusters and b) the geometry of two spherical clusters.

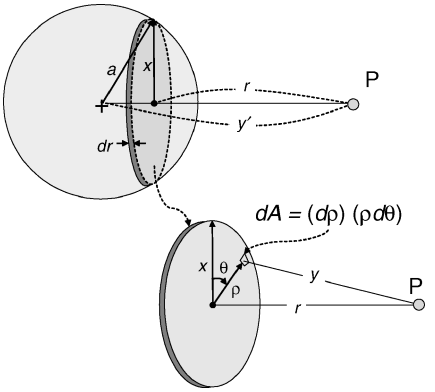

Fig. 2 Representative disk of differential thickness dr in spherical cluster A and the planar coordinate system.

d_{ij} in Eq. (1) and $U(y)$ being the LJ potential between the molecule P ($= i$) and the molecule dAdr ($= j$), the two-dimensional interaction potential [$E_{\text{M-D}}(x, r)$] between P and the disk is derived by integrating the LJ potential over the entire disk of radius x,

$$\begin{aligned} E_{\text{M-D}}(x,r) &= m_{A\rho} \int_0^x U(y)\Big|_{y=\sqrt{\rho^2+r^2}} \cdot \rho d\rho \int_0^{2\pi} \mathrm{d}\theta \\ &= 2\pi m_{A\rho} \left\{ C_1 \left[\frac{1}{10r^{10}} - \frac{1}{10(r^2+x^2)^5} \right] \right. \\ &\quad \left. - C_2 \left[\frac{1}{4r^4} - \frac{1}{4(r^2+x^2)^2} \right] \right\} \end{aligned} \tag{3}$$

where $m_{A\rho}$ measures the number of molecules per unit area on the disk. In the case that P is very close to the disk, $r \ll x$, Eq. (3) reduces to

$$E_{\text{M-D};\, r \ll x}(r) = 2\pi m_{A\rho} \left(C_1 \big/ 10r^{10} - C_2 \big/ 4r^4 \right) \tag{4}$$

Equation (4) indicates that the repulsive and attractive indices in the molecular-to-disk potential sensitively change to a 10–4 relation, in contrast to the original 12–6 (LJ) relation, as the distance between P and the disk is very small compared to x. Smaller values of the attractive and repulsive indices in the cluster potential imply a shorter equilibrium distance and a shallower potential-well depth than the LJ potential. This is because of the larger mass of clusters

as molecules congregate into a certain shape, forming a heavier body that pulls the surrounding molecules closer in approaching mechanical equilibrium.

The molecule-to-sphere potential can be derived by integrating $E_{\text{M-D}}$ in Eq. (3) for a disk of thickness (dr) over the entire sphere with r ranging from $(y'-a)$ to $(y'+a)$, with the relation of $x^2=\lfloor a^2-(y'-r)^2\rfloor$ placed in the integrand. Thus, the net interaction energy for a molecule P at a distance y' away from a sphere is

$$E_{\text{M-S}}(y')=\int_{y'-a}^{y'+a}E_{\text{M-D}}(x,r)\Big|_{x=\sqrt{a^2-(y'-r)^2}}\cdot m_{\text{Ar}}\,\mathrm{d}r$$
$$=2\pi m_A\left\{-\frac{C_1}{10}\left[\frac{1}{9(y'+a)^9}-\frac{1}{9(y'-a)^9}-\frac{1}{8y'(y'+a)^8}+\frac{1}{8y'(y'-a)^8}\right]+\frac{C_2}{4}\left[\frac{1}{3(y'+a)^3}-\frac{1}{3(y'-a)^3}-\frac{1}{2y'(y'+a)^2}+\frac{1}{2y'(y'-a)^2}\right]\right\} \tag{5}$$

where m_A $(=m_{\text{Ar}}\times m_{A\rho})$ is the number density of molecules per unit volume in sphere A. The pair force between the molecule to sphere can also be derived in a similar way from the relation $F_{\text{M-S}}(y')=-\mathrm{d}E_{\text{M-S}}(y')/\mathrm{d}y'$. The result is

$$F_{\text{M-S}}(y')=-2\pi m_A\left\{\frac{C_1}{10}\left[\frac{1}{(y'+a)^{10}}-\frac{1}{(y'-a)^{10}}-\frac{1}{y'(y'+a)^9}+\frac{1}{y'(y'-a)^9}-\frac{1}{8y'^2(y'+a)^8}+\frac{1}{8y'^2(y'-a)^8}\right]-\frac{C_2}{4}\left[\frac{1}{(y'+a)^4}-\frac{1}{(y'-a)^4}-\frac{1}{y'(y'+a)^3}+\frac{1}{y'(y'-a)^3}-\frac{1}{2y'^2(y'+a)^2}+\frac{1}{2y'^2(y'-a)^2}\right]\right\} \tag{6}$$

Equations (5) and (6) show that the molecule-to-sphere potential and the interaction force is not only proportional to the number density of molecules in the sphere but also depends on the size of the sphere.

For the case that the molecule is very close to the sphere cluster, that is, $d\ll a$ with $d(=y'-a)$ being the distance between P and the surface of sphere A, the potential that is simplified from Eq. (5) becomes

$$E_{\text{M-S},d\ll a}=\pi m_A\left(C_1/45d^9-C_2/6d^3\right) \tag{7}$$

The 10–4 relation of the potential function Eq. (4) further evolves into a 9–3 relation in Eq. (7) in transit from the molecule to disk to the molecule to sphere. The corresponding force is therefore given by

$$F_{\text{M-S},d\ll a}=\pi m_A\left(C_1/5d^{10}-C_2/2d^4\right) \tag{8}$$

The equilibrium length, which is defined here as the distance between a molecule and the surface of a large spherical cluster at a small distance apart, is $(2C_1/5C_2)^{1/6}$. The maximum attractive force therefore is $-3\pi m_A C_2/10(C_1/C_2)^{2/3}$, at a distance of $(C_1/C_2)^{1/6}$ between the molecule and the surface of the sphere. A cluster array with $d\ll a$ is termed tightly compacted in this work.

For the other extreme that $a\ll d$, for loosely compacted cluster arrays, the Taylor-series expansion of Eq. (5) in terms of (a/y') yields

$$E_{\substack{\text{M-S}\\ a\ll d}}(y')=\left(4\pi a^3 m_A/3\right)\left(C_1/y'^{12}-C_2/y'^6\right) \tag{9}$$

The value of $4\pi a^3 m_A/3$ is the number of molecules in the sphere A. The LJ potential is thus retrieved by letting the number of molecule in the sphere be unity (1).

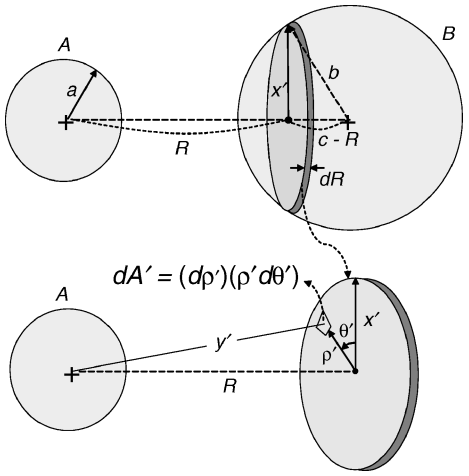

Fig. 3 Representative disk of differential thickness dR in spherical cluster B and the planar coordinate system.

Sphere-to-Sphere Potential

Figure 3 illustrates the coordinate system employed in deriving the potential between sphere A and sphere B. Similar to the molecule-to-disk potential, the disk-to-sphere potential $E_{\text{D-S}})$ can be derived by replacing y' in Eq. (5) by $(\rho'^2+R^2)^{1/2}$ and integrating $E_{\text{M-S}}$ over the entire disk with $\rho'\in[0,x']$ and $\theta'\in[0,2\pi]$. Employing the identity

$$\int_0^{x'}\frac{\rho'}{\left(\sqrt{R^2+\rho'^2}\pm a\right)^n}\,\mathrm{d}\rho'=\int_0^{x'}\frac{\rho'\sqrt{R^2+\rho'^2}}{\sqrt{R^2+\rho'^2}\left(\sqrt{R^2+\rho'^2}\pm a\right)^n}\,\mathrm{d}\rho' \tag{10}$$

in the integration, all terms can be integrated by parts, resulting in the expression for the disk-to-sphere potential:

$$E_{\text{D-S}}(x',R)=m_{B\rho}\int_0^{x'}E_{\text{M-S}}(y')|_{y'=\sqrt{\rho'^2+R^2}}\cdot\rho'\,\mathrm{d}\rho'\int_0^{2\pi}\mathrm{d}\theta'$$
$$=4\pi^2 m_A m_{B\rho}\left\{\frac{C_1}{720}\left[\frac{\bar R}{(\bar R+a)^8}-\frac{\bar R}{(\bar R-a)^8}-\frac{R}{(R+a)^8}+\frac{R}{(R-a)^8}\right]-\frac{C_1}{630}\left[\frac{1}{(\bar R+a)^7}-\frac{1}{(\bar R-a)^7}-\frac{1}{(R+a)^7}+\frac{1}{(R-a)^7}\right]-\frac{C_2}{24}\left[\frac{\bar R}{(\bar R+a)^2}-\frac{\bar R}{(\bar R-a)^2}-\frac{R}{(R+a)^2}+\frac{R}{(R-a)^2}\right]+\frac{C_2}{12}\left[\frac{1}{\bar R+a}-\frac{1}{\bar R-a}-\frac{1}{R+a}+\frac{1}{R-a}\right]\right\} \tag{11}$$

where $m_{B\rho}$ is the number density of molecules per unit area on the disk (of thickness dR) located within sphere B and $\bar R=\sqrt{(R^2+x'^2)}$.

The $E_{\text{D-S}}$ function is now integrated in the domain of R from $(c-b)$ to $(c+b)$, with x' replaced by $[b^2-(c-R)^2]^{1/2}$ in all terms. Rearrangements such as

$$\int_{c-b}^{c+b}\frac{\sqrt{2cR-(c^2-b^2)}}{\left[\sqrt{2cR-(c^2-b^2)}\pm a\right]^n}\,\mathrm{d}R$$
$$=\int_{c-b}^{c+b}\frac{2cR-(c^2-b^2)}{\sqrt{2cR-(c^2-b^2)}\left[\sqrt{2cR-(c^2-b^2)}\pm a\right]^n}\,\mathrm{d}R \tag{12}$$

in parallel to the preceding treatment, are required to render the close-form result via integrations by parts. The resulting sphere-to-sphere potential is thus

$$E_{\text{S-S}} = m_{\text{BR}} \int_{c-b}^{c+b} E_{\text{D-S}}(x', R)\Big|_{x'=\sqrt{b^2-(c-R)^2}} \cdot \mathrm{d}R$$

$$= \pi^2 m_A m_B \left\{ \frac{C_1}{37{,}800c} \left[\frac{c^2+7gc+G}{(c+g)^7} + \frac{c^2-7gc+G}{(c-g)^7} - \frac{c^2+7hc+H}{(c+h)^7} - \frac{c^2-7hc+H}{(c-h)^7} \right] - \frac{C_2}{6} \left[\frac{2ab}{c^2-g^2} + \frac{2ab}{c^2-h^2} + \ell_n \frac{c^2-g^2}{c^2-h^2} \right] \right\} \quad (13)$$

where $m_B = m_{B\rho} \times m_{\text{BR}}$, $g = a+b$, $h = a-b$, $G = 6a^2+6b^2+42ab$, and $H = 6a^2+6b^2-42ab$. Equation (13) indicates the net interaction energy between two spheres is proportional to not only the number densities of molecules in the spheres but also the sizes (e.g., radius) of the spheres.

The interaction force between two spherical clusters is evaluated from the gradient of Eq. (13),

$$F_{\text{S-S}} = -\frac{\mathrm{d}E_{\text{S-S}}}{\mathrm{d}c}$$

$$= \pi^2 m_A m_B \left\{ \frac{C_1}{37{,}800c^2} \left[\frac{6c^3+48gc^2+8Gc+gG}{(c+g)^8} + \frac{6c^3-48gc^2+8Gc-gG}{(c-g)^8} - \frac{6c^3+48hc^2+8Hc+hH}{(c+h)^8} - \frac{6c^3-48hc^2+8Hc-hH}{(c-h)^8} \right] - \frac{C_2 c}{3} \left[\frac{2ab}{(c^2-g^2)^2} + \frac{2ab}{(c^2-h^2)^2} - \frac{1}{c^2-g^2} + \frac{1}{c^2-h^2} \right] \right\} \quad (14)$$

Equations (13) and (14) are the general expressions for the pair potential and force between two spherical clusters.

Assuming two large spheres with a small distance apart, that is, $d \ll a$ and $d \ll b$ with $d = c-(a+b)$ referring to the distance between the surfaces of two spheres, the pair potential is deduced from Eq. (13):

$$E_{\text{S-S}(d \ll a,b)} = \frac{\pi^2 m^2 ab}{a+b} \left(\frac{C_1}{1260d^7} - \frac{C_2}{6d} \right) \quad (15)$$

Note that the 9–3 relation of the molecule-to-sphere potential finally evolves into a 7–1 relation for the sphere-to-sphere potential. It is clearly shown that the interaction energy is proportional to the radii of both spheres. The net force between the two spheres is therefore

$$F_{\text{S-S}(d \ll a,b)} = \frac{\pi^2 m^2 ab}{a+b} \left(\frac{C_1}{180d^8} - \frac{C_2}{6d^2} \right) \quad (16)$$

It is also proportional to the radii of the spheres and decays as d^{-8} for the repulsive force and d^{-2} for the attractive force.

For $a = b$ and $m_A = m_B$, the potential Eq. (13) and the force Eq. (14) respectively become

$$E_{\text{S-S}(a=b)} = \pi^2 m^2 \left\{ \frac{C_1}{37{,}800c} \left[\frac{c^2+54a^2+14ac}{(c+2a)^7} + \frac{c^2+54a^2-14ac}{(c-2a)^7} + \frac{2c^2-60a^2}{c^7} \right] - \frac{C_2}{6} \left[\frac{2a^2}{c^2-4a^2} + \frac{2a^2}{c^2} + \ell_n \frac{c^2-4a^2}{c^2} \right] \right\} \quad (17)$$

and

$$F_{\text{S-S}(a=b)} = \pi^2 m^2 \left\{ \frac{C_1}{37{,}800c^2} \left[\frac{6c^3+96ac^2+432a^2c+108a^3}{(c+2a)^8} + \frac{6c^3-96ac^2+432a^2c-108a^3}{(c-2a)^8} - \frac{12c^2-480a^2}{c^7} \right] - \frac{C_2}{3} \left[\frac{2a^2c}{(c^2-4a^2)^2} + \frac{2a^2}{c^3} - \frac{c}{c^2-4a^2} + \frac{1}{c} \right] \right\} \quad (18)$$

The number density of molecules m is replaced form_A and m_B in the preceding two equations.

For $a = b$ and $d \ll a$, the asymptotic limit of the potential is obtained from Eq. (17):

$$E_{\text{S-S}(a=b,d \ll a)} = \pi^2 m^2 a \left(C_1 \big/ 2520d^7 - C_2/12d \right) \quad (19)$$

The same result can also be obtained by letting $a = b$ in Eq. (15). Similarly, the asymptotic limit of the force is

$$F_{\text{S-S}(a=b,d \ll a)} = \pi^2 m^2 a \left(C_1 \big/ 360d^8 - C_2 \big/ 12d^2 \right) \quad (20)$$

Letting the force in Eqs. (18) and (20) be zero, respectively, yields the same equilibrium length between the surfaces of two close large spherical clusters $(C_1/30C_2)^{1/6}$. The maximum attractive force is $-3\pi^2 m^2 a C_2/(2C_1/15C_2)^{1/3}$ as the distance between the surfaces of the two spheres reaches $(2C_1/15C_2)^{1/6}$. Recall that the equilibrium length is $(2C_1/5C_2)^{1/6}$ for a molecule and the surfaces of a close-by large spherical cluster and is $(2C_1/C_2)^{1/6}$ for the LJ potential for a molecule.

The LJ potential can be deduced from the case that $a = b$ and $a \ll d$ although the derivation is tedious. Expanding the Taylor series for the first two terms and the last term on the right-hand side of Eq. (14) and neglecting the relatively higher-order terms in (a/c) results in

$$E_{\text{S-S}(a=b,d \gg a)} = (16\pi^2 a^6 m^2/9) \left(C_1 \big/ c^{12} - C_2 \big/ c^6 \right) \quad (21)$$

Because $4\pi a^3 m/3$ is simply the number of molecules in a sphere, the preceding pair potential is identical to the LJ potential as $4\pi a^3 m/3 = 1$.

Molecule-to-Flat-Surface Potential

A surface can be treated as a planar cluster made of molecules. In performing the molecular dynamics simulation, this approach allows us to model the surface bounding the molecular motion as a participating piece (cluster) in the computational domain. The need for specifying the kinematic conditions describing the collisions between the molecules and a physical boundary is thus removed. Comparing Figs. 2 and 4a, the molecule-to-surface potential can easily be obtained by integrating the molecule-to-disk potential $E_{\text{M-D}}(x', z')$

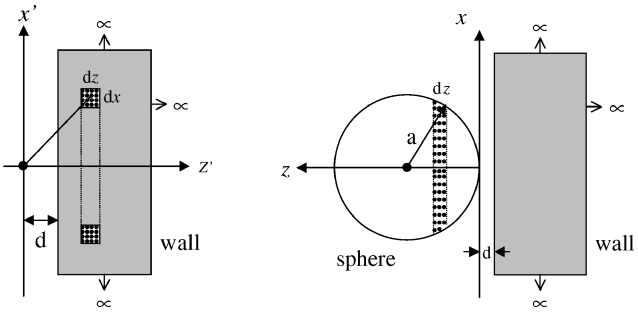

a) Molecule-to-wall **b) Sphere-to-wall**

Fig. 4 Coordinates systems for molecule to wall and spherical cluster to wall.

with $x' \to \infty$ over the domain $z' \in [d, \infty]$. The result is

$$E_{\text{M-W}}(d) = \int_d^{\infty} E_{\text{M-D}}(x', z')\Big|_{x'=\infty} \mathrm{d}z' = \pi m_w \left\{ \frac{C_1}{45d^9} - \frac{C_2}{6d^3} \right\} \tag{22}$$

where m_W is the number density of molecules in the wall and d is the distance between the molecule and the surface of the wall. Note that Eq. (22) is identical to Eq. (7), which is the extreme case that a molecule interacts with a very large sphere. This is because a flat surface is a limit of the surface of a sphere as the radius of the sphere approaches infinite. As a result, the expression of the interaction force between a molecule and a flat surface is the same as Eq. (8).

Note that the simple expression shown by Eq. (22) results from the assumption that the wall is composed of the same molecule. For walls involving different molecules, which will be the case in most applications, Lorentz–Berthelot mixing rules[17] need to be applied while the cluster concept remains the same.

Sphere-to-Flat Surface Potential

The pair potential of a sphere with the flat surface of an infinite thick and long wall can be derived in the same manner as described in the Sphere-to-Sphere Potential section. Replacing d in Eq. (22) with $(d + z)$ and integrating $E_{\text{M-S}}$ over the entire disk with $\rho' \in [0, x']$ and $\theta \in [0, 2\pi]$ results in the disk-to-flat surface potential

$$E_{\text{D-W}}(x, z, d) = m_D \int_d^{\infty} E_{\text{M-W}}(d')\Big|_{d'=d+z} \rho' \,\mathrm{d}\rho \int_0^{2\pi} \mathrm{d}\theta$$

$$= \pi^2 m_w m_D \left\{ \frac{C_1 x^2}{45(d+z)^9} - \frac{C_2 x^2}{6(d+z)^3} \right\} \tag{23}$$

in which m_D is the number density of molecules in the disk, d is the distance between the surfaces of the wall and the sphere, and $(d + z)$ is the distance between the disk and the wall surface. The sphere-to-flat surface potential can be obtained by integrating the $E_{\text{D-W}}$ potential,

$$E_{\text{S-W}}(a, d) = \int_0^{2a} E_{\text{D-W}}(x, z, d)\Big|_{x=\sqrt{a^2-(a-z)^2}} m_z \,\mathrm{d}z$$

$$= \pi^2 m_w m_s \left\{ \frac{C_1}{7560} \left[\frac{8a+d}{(2a+d)^7} + \frac{6a-d}{d^7} \right] \right.$$

$$\left. - \frac{C_2}{6} \left[-\frac{4a+3d}{2(2a+d)} + \frac{2a+3d}{2d} - \ell_n \frac{2a+d}{d} \right] \right\} \tag{24}$$

where $m_a (= m_D \times m_Z)$ and a are the number density of molecules and the radius of the sphere, respectively. The value of the force $F_{\text{S-W}}(a, d)$ for a sphere near a flat surface is

$$F_{\text{S-W}}(a, d) = -\frac{\partial E_{\text{S-W}}(a, d)}{\partial d} = \pi^2 m_w m_a \left\{ \frac{C_1}{3780} \left[\frac{27a+3d}{(2a+d)^8} \right.\right.$$

$$\left. + \frac{21a-3d}{d^8} \right] - \frac{C_2}{6} \left[\frac{3a+d}{(2a+d)^2} + \frac{a-d}{d^2} \right] \Bigg\} \tag{25}$$

For $d \ll a$, Eq. (24) reduces to

$$E_{\text{S-W},d \ll a}(a, d) = \pi^2 m_w m_a a \left(C_1 \Big/ 1260d^7 - C_2/6d \right) \tag{26}$$

which is the extremely case of the interaction between two spheres, see Eq. (15) with $b \to \infty$. For the other special case that $a \ll d$, the Taylor-series expansion of Eq. (24) in terms of a/d gives

$$E_{\text{M-W},a \ll d}(d) = \pi m_w \left(4\pi a^3 m_a \Big/ 3 \right) \left(C_1 \Big/ 45d^9 - C_2 \Big/ 6d^3 \right) \tag{27}$$

Letting the number of molecules in the sphere $4\pi a^3 m_a/3$ be one (1), the preceding potential is basically the same as Eq. (22) for the interaction of a molecule with a flat surface.

The indices describing the attractive and repulsive forces decrease as the dimensionality of the cluster increases, from the 12–6 relation for molecules-to-molecule (zero dimension for both), the 10–4 relation for molecule-to-flat-surface (dimension of 2 for flat surfaces), the 9–3 relation for molecule-to-sphere (dimension of 3 for spheres), and the 7–1 relation for sphere-to-sphere (dimension of 3 for both). Under the same number density of molecules in the cluster, a higher dimension of the cluster implies more molecules involved, and, consequently, the cluster becomes heavier. A heavier cluster pulls the neighboring molecules closer in approaching mechanical equilibrium, which, in turn, is reflected by smaller values of the attractive and repulsive indices.

Comparisons

The pair potential and force strongly depend on the size of the dimension of clusters as well as the distance between the two clusters. For ease of numerical presentation in comparing the potential and force between clusters, it is convenient to express them in a dimensionless form. In view of the similarity among the potential functions given by Eqs. (1), (7), (15), and (27), the following dimensionless form for the pair potentials is introduced

$$\bar{E}(D) = E(D)/E^* = 1/\alpha D^{\xi} - 2/\beta D^{\eta} \tag{28}$$

where $E^* = AE_0 d_0^{6-\eta}$ and $D = d/d_0$ with $d_0 = (2C_1/C_2)^{1/6}$ being the equilibrium position between two molecules. The newly introduced five parameters, A, α, β, ξ, and η, are summarized in Table 1 for clusters of the various shapes. Accordingly, the corresponding forces are expressed as

$$\bar{F}(D) = F(D)/F^* = \xi/\alpha D^{\xi+1} - 2\eta/\beta D^{\eta+1}$$

$$\text{where} \qquad F^* = E^*/d_0 \tag{29}$$

Figure 5 displays the dimensionless potentials between a molecule and a sphere cluster (Fig. 5a), two spheres of the same size ($a = b$) (Fig. 5b), and two spheres of different sizes ($a \neq b$ and $a = 10$ nm) (Fig. 5c). Equation (5) is employed in obtaining Fig. 5a whereas Eq. (13) is employed in obtaining Figs. 5b and 5c. For comparison, the LJ potential is included in Fig. 5a. Those results are calculated with the values of $C_1 = 10^{-26}$ J · nm^{12}, $C_2 = 10^{-23}$ J · nm^6, and $m = 31.6$ atoms/nm^3. The value of the number density employed here is based on a tightly packed solid, and the equilibrium length between two molecules is $d_0 = 0.355$ nm. Recall that the relations between the repulsion and attraction with respect to the distance d are 12–6 for two molecules, 9–3 for a molecule and a sphere, and 7–1 for two spheres. Obviously, the interaction potentials of molecule to sphere and sphere to sphere would decay very much slower than the intermolecular potential. The distance dependence of the interaction is seen in Figs. 5a–5c. The equilibrium length d, which depends on the size of a cluster, is calculated to be 0.2714 nm for a molecule and a large sphere, assuming $d \ll a$, and 0.1794 nm for the two large spheres, assuming $d \ll a, b$. They are the same as those calculated directly from Eqs. (8) and (16). On the other hand, the equilibrium lengths for each type of the clusters are close. For instance, those computed for the two spheres of the same size are 0.1863 nm for $a = 1$ nm, 0.1801 nm for $a = 10$ nm, 0.1795 nm for $a = 100$ nm, and 0.1794 nm for $a = 1$ μm.

Table 1 Cluster potentials $\bar{E}$ and interaction forces $\bar{F}$: $\bar{E}(D) = E(D)/E^* = 1/\alpha D^{\xi} - 2/\beta D^{\eta}$, $\bar{F}(D) = F(D)/F^* = \xi/\alpha D^{\xi+1} - 2\eta/\beta D^{\eta+1}$, where $E^* = AE_0 d_0^{6-\eta}$, $D = d/d_0$, $d_0 = (2C_1/C_2)^{1/6}$

Cluster type	A	α	β	ξ	η
Molecule-to-molecule (LJ)	1	1	1	12	6
Molecule-to-sphere	πa	45	6	9	3
Sphere-to-sphere	$\dfrac{\pi^2 m^2 ab}{a+b}$	1260	6	7	1
Molecule-to-flat surface	πm_w	45	6	9	3
Sphere-to-flat surface	$a\pi^2 m_w m_a$	1260	6	7	1

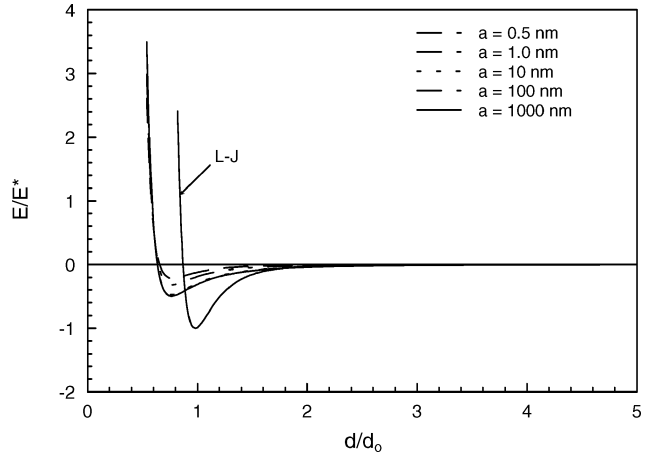

a)

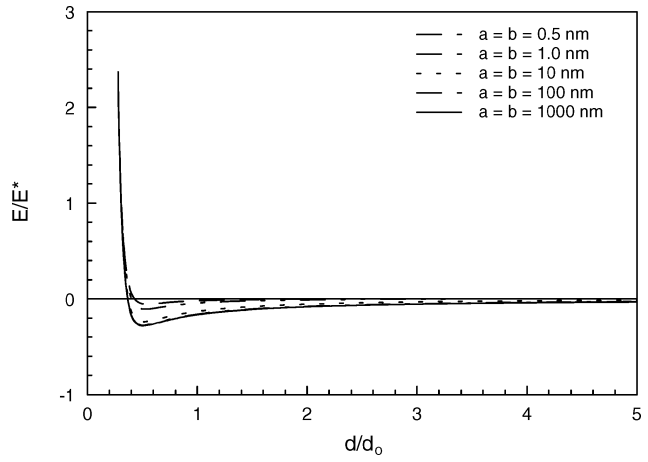

b)

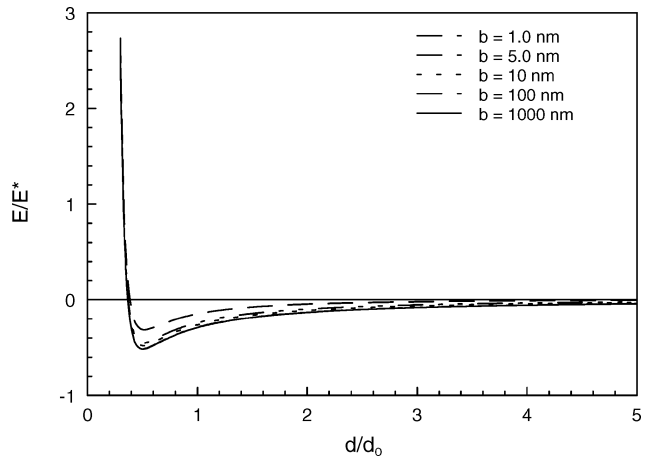

c)

Fig. 5 Normalized potentials between a) a spherical cluster and atom, b) two spherical clusters of same size, and c) two spherical clusters of different sizes: $a = 10$ nm and $b = 1 - 1000$ nm.

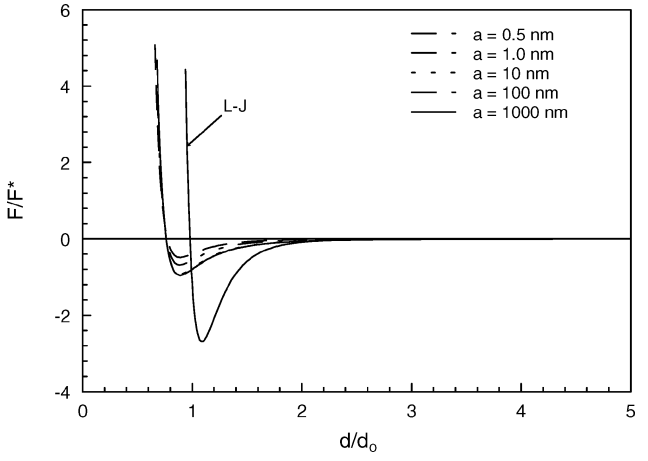

a)

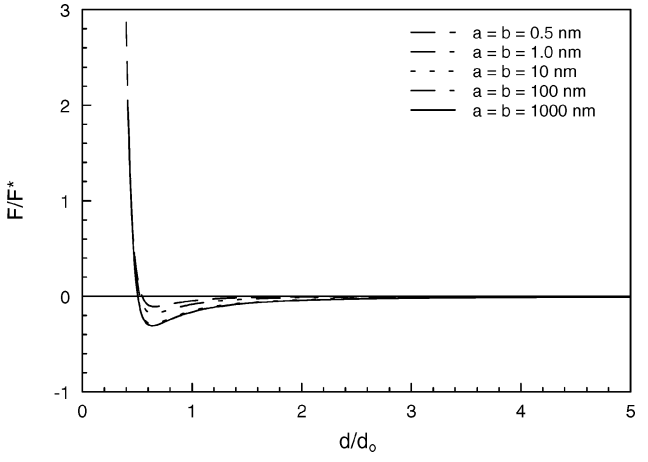

b)

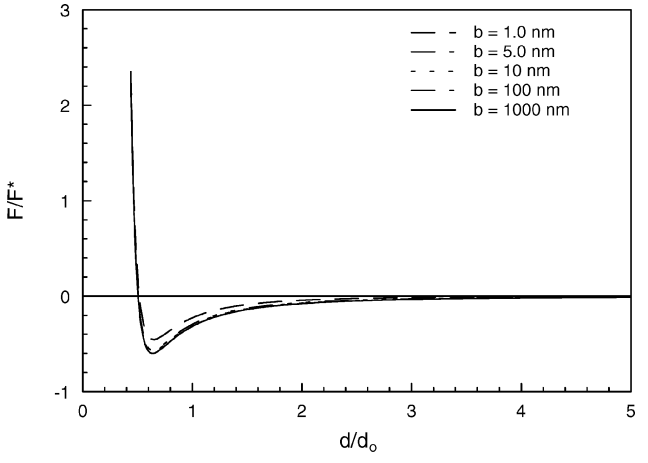

c)

Fig. 6 Normalized interaction forces between a) a spherical cluster and atom, b) two spherical clusters of same size, and c) two spherical clusters of different sizes: $a = 10$ nm and $b = 1 - 1000$ nm.

Figure 6 displays the corresponding nondimensional interaction forces. The maximum attractive force is -1.895×10^{-11} N for the two molecules at the distance $d_s = 0.3935$ nm (LJ), -2.977×10^{-11} N for a molecule and a large sphere ($a = 1$ μm) at the surface distance 0.3159 nm as shown in Fig. 6a, and -0.121×10^{-7} N for the two spheres of equal radii $a = b = 1$ μm at the surface distance 0.2260 nm, Fig. 6b. As shown in Fig. 6a, the interaction force between two molecules (LJ potential) decays quite fast as the distance dependences of the repulsive and attractive forces are d^{-13} and d^{-7}, respectively. For instance, the ratio of the net force at the distance $2.6d_0$ to the maximum negative force occurring at d_s is about 0.0055. Accordingly, the contribution from the molecules located at the distance exceeding approximately $2.6d_0$ can be considered insignificant and thus is treated as the threshold value of the cutoff radius for improving the numerical efficiency.[1,2] The clusters, on the other hand, have a longer range of influence, with the effective distance d extending well beyond $2.6d_0$ ($d > 2.6d_0$), especially for those clusters of higher dimensions. For the interaction between a molecule and a spherical cluster, for instance, the required distance d for the ratio of the force to the maximum negative force is less than

0.0055 is $3.2d_0$ for the sphere of radius 1 nm, $3.7d_0$ for the sphere of radius 10 nm, $3.8d_0$ for the sphere of radius 100 nm, and $3.8d_0$ for the sphere of radius 1 μm. The required distance should even be larger for the interaction between two spherical clusters of the same size; they are $4.2d_0$ for the spheres of radius 1 nm, $7.9d_0$ for the spheres of radius 10 nm, $9.7d_0$ for the spheres of radius 100 nm, $9.9d_0$ for the spheres of radius 1 μm, and $10.0d_0$ for the spheres of radius 10 μm. For the interaction between two spherical clusters of different size, for which the radius of one of the spheres is 10 nm and the other varies for example, the required distance is $5.4d_0$ for $b = 1$ nm, $7.9d_0$ for $b = 10$ nm, $8.7d_0$ for $b = 100$ nm, $8.8d_0$ for $b = 1$ μm, and $8.8d_0$ for $b = 10$ μm. The threshold values of the cutoff radius for numerical analysis are respectively around $4d_0$, $10d_0$, and $9d_0$ for the preceding three cases. Although the threshold value of the cutoff d larger than that required for the two molecules, only one cluster on each side of the cluster is needed in the numerical simulation because of the size of the spherical clusters. For instance, the maximum cutoff distance of $4d_0$ for the interaction between a molecule and a sphere of radius 1 nm is 1.136 nm, while the next closest sphere to the molecule is at least 3 nm apart. The worst case is that four molecules are needed to be involved with a cluster in the region that transits molecules to very large clusters. Overall speaking, cluster dynamics requires much less computational time than molecule dynamics.

In multiscale modeling, a robust model should consist of molecules and clusters of different sizes. Because the molecule-to-sphere potential Eq. (7) provides a transition from molecules to clusters and the sphere-to-sphere cluster potential Eq. (15) is size dependent, the multiscale model can vary from single molecule, small clusters (few molecules) to very large clusters (thousands of molecules). Unlike millions of molecules often required in MD simulation, the two potentials Eqs. (7) and (15) developed in this work along with the LJ potential could provide a better tool for multiscale modeling with molecules and spherical clusters.

Validity of the asymptotic expressions shown by Eqs. (19) and (20), as compared to the full expressions shown by Eqs. (17) and (18), is noteworthy. The central distance c in Eqs. (17) and (18), in relation to the surface distance d in Eqs. (19) and (20), is replaced by $c = d + 2a$. Normalizing both forms of the cluster potential energy by $E^* = C_1 m^2 \pi^2 / d_0^6$ [for Eqs. (17) and (19)] and the interaction force by $F^* = C_1 m^2 \pi^2 / d_0^7$ [for Eqs. (18) and (20)], with $C_2 = 2C_1/d_0^6$ and d_0 the equilibrium distance of the classical LJ potential, comparisons of Eqs. (17) and (19) (cluster potential) and Eqs. (18) and (20) (interaction force) are shown in Fig. 7. The results depend on only two parameters A and D. Major differences between the full forms [Eqs. (17) and (18)] and the asymptotic forms [Eqs. (19) and (20)] occur for clusters with a small value of A $(= a/d_0)$. As the cluster radius a is small comparing to the equilibrium distance d_0, which includes tightly packed assemblies as a special case, therefore, full expressions of the cluster potential and interaction force must be employed. As the value of A becomes large, $A = 100$ shown by Figs. 7b and 7d, asymptotic forms can be used in place of the full forms because of the coalescence of the potential and force curves.

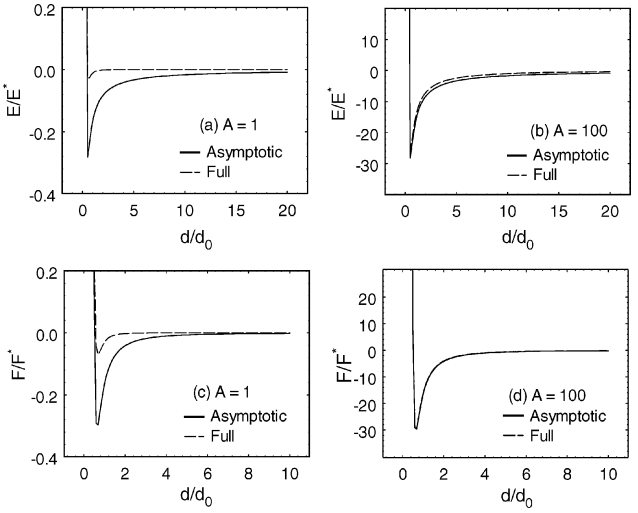

Fig. 7 Comparison of the asymptotic and full expressions for the spherical cluster potentials.

Dynamic Simulations

The cluster potentials thus derived are readily implemented into any computer code employing the MD simulation. Especially for loosely packed assemblies in microscale where the cluster radius is small compared to the distance between clusters, the required change in the code only involves the exponents describing attractions and repulsions (see Table 1), which depend only on the geometrical configuration(s) of the cluster(s) involved.

To better describe the unique features in cluster dynamics, we model the one-dimensional interactions among N identical spherical clusters. Full expression of the force, with c measuring the central distance between two clusters, shall be used for the sake of generality. Nondimensional forms of the equations of motion can be written as

$$\ddot{X}_i = \frac{\mathrm{d}^2 X_i}{\mathrm{d}\tau^2} = \sum_{\substack{j=1 \\ j\neq i}}^{N} \bar{F}_{ij}, \qquad \ddot{X}_j = \frac{\mathrm{d}^2 X_j}{\mathrm{d}\tau^2} = -\sum_{\substack{j=1 \\ j\neq i}}^{N} \bar{F}_{ij}$$

$$\text{for} \qquad i, j = 1, 2, \ldots, N$$

where

$$X_i = x_i/d_0, \qquad V_i = \dot{x}_i \Big/ \left(d_0^3 m\pi \Big/ \sqrt{M/E_0}\right)$$

$$\tau = t \Big/ \sqrt{M \Big/ \left(E_0 d_0^4 m^2 \pi^2\right)}, \qquad A = a/d_0, \qquad D = |x_j - x_i|/d_0$$

and

$$\begin{aligned}\bar{F}_{ij} = [&-1728A^4D^{14} + 72A^2D^{16} - D^{18} \\ &- 40320A^8D^{10}(3 + 20D^6) + 1344A^6D^{12}(-9 + 25D^6) \\ &+ 1310720A^{18}(1 + 105D^6) + 64512A^{10}D^8(6 + 125D^6) \\ &- 172032A^{12}D^6(7 + 250D^6) - 294912A^{16}D^2(9 + 700D^6) \\ &+ 147456A^{14}D^4(16 + 875D^6)]/[1575D^9(D^2 - 4A^2)^8] \end{aligned} \quad (30)$$

$\bar{F}_{ij}$ is the nondimensional force from cluster j to cluster i, d_0 is the equilibrium distance of the LJ potential, $E_0 = C_2^2/(4C_1)$ is the well depth of the LJ potential, and dots represent derivatives with respect to time.

Equation (30) represents a set of nonlinearly coupled ordinary differential equations to be solved for the cluster displacements X_i and velocities V_i in the time history. The subroutine for solving the stiff ordinary differential equations, IVPAG in the International Mathematical and Statistical Library package, is employed here for its popular use and easy access. We chose the fifth-order backward-differentiation formulas (often called Gear's stiff method) in the implicit differencing scheme. The norm of the local error (at each time step) is controlled such that the global error (over all time steps) is ensured to be less than 10^{-6}. The virial theorem[11,12] calculates the transport properties from the cluster displacements X_i and velocities V_i evaluated numerically at each time step. Heat flux q and pressure p, for example, can be calculated from

$$Q = \frac{q}{q_0} = \frac{1}{N}\sum_{i=1}^{N} \overline{\left(E_i^P + E_i^K\right)V_i}, \qquad \Sigma = \frac{p}{p_0}$$

$$= -\frac{1}{N}\left[2\left(\frac{c_0}{d_0}\right)^{12} \sum_{i=1}^{N} \overline{V_i V_i} + \sum_{i=1}^{N} \overline{\bar{F}_{ij}(X_i - X_j)}\right]$$

where

$$q_0 = \frac{(m\pi)^3 C_1 C_2}{2Sc_0^3 (C_1/C_2)^{\frac{1}{6}} \sqrt{4MC_1}}, \qquad p_0 = \frac{C_1 (m\pi)^2}{2Sc_0^6 (C_1/C_2)^{\frac{1}{6}}} \tag{31}$$

where E_i^P is the potential energy of cluster j exerting on cluster i, $j = 1, 2, \ldots, N$, but $j \neq i$, resulting from Eq. (17) with c being the central distance between clusters i and j, and E_i^K is the kinetic energy of cluster i, calculated from $V_i^2/2$ in the nondimensional form. The reference values, q_0 and p_0 in Eq. (32), result from the process making the virial theorem nondimensional. They fall out naturally, in exactly the same fashions as those shown in Eq. (31) for the reference values of displacement, velocity, and time. Again, the relations for the LJ potential are introduced in deriving Eq. (32), including the coefficients C_1 and C_2, as well as the equilibrium position d_0 shown after Eq. (2). Surface area S refers to the physical domain across which thermal energy and momentum take place. It has been absorbed in the reference value of q_0 and p_0 in the present one-dimensional formulation, but a multidimensional formulation is more suitable for studying the heat flux and stresses caused by involvement of the area. When a multidimensional formulation is attempted, not only multiple degrees of freedom (two or three dimensional) need to be accommodated in describing the cluster motion, but all of the reference values defined in Eqs. (30) and (31) need to be redetermined.

Fundamental behavior of cluster dynamics is illustrated by a 10-cluster array shown in Fig. 8, where the oscillatory patterns of the first cluster is focused under the various forms of the cluster/molecular potentials. The motion is set forth under the following initial conditions:

$$X_i(0) \equiv \frac{x_i(0)}{d_0} = \begin{cases} 1.06(i-1), & i = 1, 2, \ldots, 10 \quad \text{(CD asymptotic and MD)} \\ 2A(i-1) \times 1.06, & i = 1, 2, \ldots, 10 \quad \text{(CD full form)} \end{cases} \tag{32}$$

which describe a 6% initial displacement over the LJ equilibrium distance d_0 between molecules (the 12-6 LJ potential), adjacent clusters (the 7–1 asymptotic form), and the surface distance (full form) of adjacent clusters. In the full-form expression in Eq. (32), $2A$ measures the minimum distance between the surfaces of two adjacent spheres of equal radius A. The assumed 6% disturbance from the equilibrium position assures that the 10 clusters stay in the array without unrecoverable separations in the dynamic response. Generally speaking, comparing to the molecular (12–6) motion, the clusters oscillate at lower frequencies with larger amplitudes, resulting from the heavier mass of clusters as numerous molecules congregate. Dynamic response for clusters employing the full-form potential, Eqs. (30) and (32), strongly depends on the cluster radius A. Under the initial conditions specified in Eq. (32), the case of $A = 5$ represents a critical stage. As $A = 5$, the dynamic response of the first cluster X_1 is still able to retain a pseudoharmonic motion, with a smaller amplitude and a lower frequency comparing to the 7–1 (asymptotic) response. The harmonic motion starts to break down as the value of A slightly increases, shown by the response curve of $A = 6$ in Fig. 8. Periodic motion can still be observed in the overall envelope, but severe local oscillations start to grow, which eventually leads to an unstable response, that is, clusters permanently leaving the array. In correspondence with the physical scales of space and time, note that $x \cong 0.18X$ (nm) and $t \cong 1.26\tau$ (ns) in Fig. 8, which apply to all results shown in this work. The system parameters, including the molecular density m in each cluster and the cluster mass M, do not affect the nondimensional responses presented in Fig. 8. These parameters only influence the stretching factors, 0.18 (for X) and 1.26 (for τ) assuming $m = 10$ molecules/cluster and $M = 66.3 \times 10^{-26}$ kg, in recovering the dimensional displacement x and time t in the physical space.

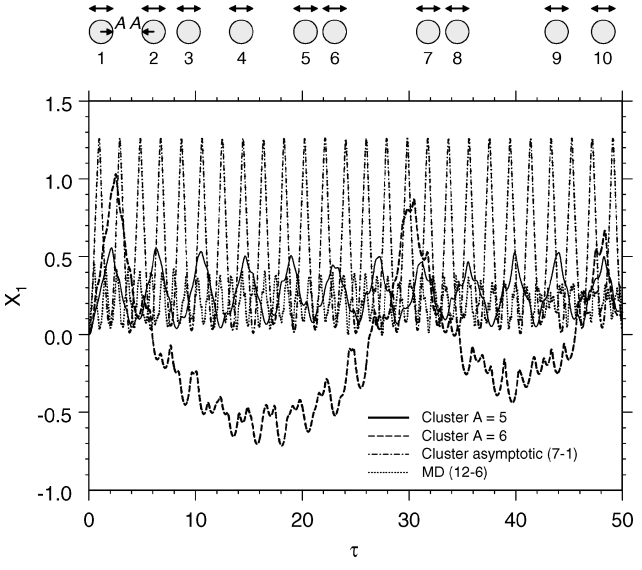

Fig. 8 Dynamics of clusters with different forms of potential.

Maxwell–Boltzmann velocity distribution is a necessary condition to examine the number of particles needed for accurate simulations.[3] In a quasi-stationary response, the time average of the particle velocity, $\bar{v}$ or $\bar{V}$ defined in Eq. (30), must follow the relation

$$\frac{\Delta N_V}{N} \equiv P = \left(\frac{M}{2\pi k_B \bar{T}}\right) \exp\left[-\frac{M\bar{v}^2}{2\pi k_B \bar{T}}\right] \times \Delta\bar{v} = \frac{\exp(-\bar{V}^2/2\bar{\theta})}{\sqrt{2\pi\bar{\theta}}} \times \Delta\bar{V} \tag{33}$$

It measures the probability of having ΔN_V clusters (among the total of N clusters) that have a time-averaged velocity within the velocity window of $(\bar{V} + \Delta\bar{V})$. Because the averaged temperature, $\bar{T}$ or $\bar{\theta} = \bar{T}/(E_0/6k_B)$ in Eq. (33), is related to the averaged velocity by

$$\tfrac{1}{2}Mv^2 = \tfrac{3}{2}k_B T, \qquad \text{or} \qquad \bar{\theta} = \bar{V}^2/3 \tag{34}$$

in a nondimensional form, the probability is a strong function of the averaged velocity $\bar{V}$. Figure 9 shows the evolution of the probability density curve as the number of clusters increases from 50 to 150. Full expression of the cluster potential with $A = 5$ in Eq. (30) is used in this simulation. A better agreement with the Maxwell–Boltzmann distribution can be achieved by the use of more clusters. In view of the exponentially increased computational time as the number of clusters increases in the numerical simulation, and the acceptable

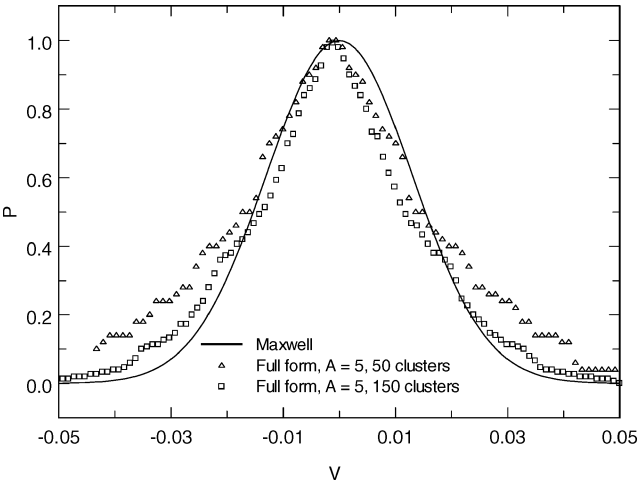

Fig. 9 Maxwell–Boltzmann velocity distribution curve and cluster arrays with 50 and 150 clusters (full expression with $A = 5$).

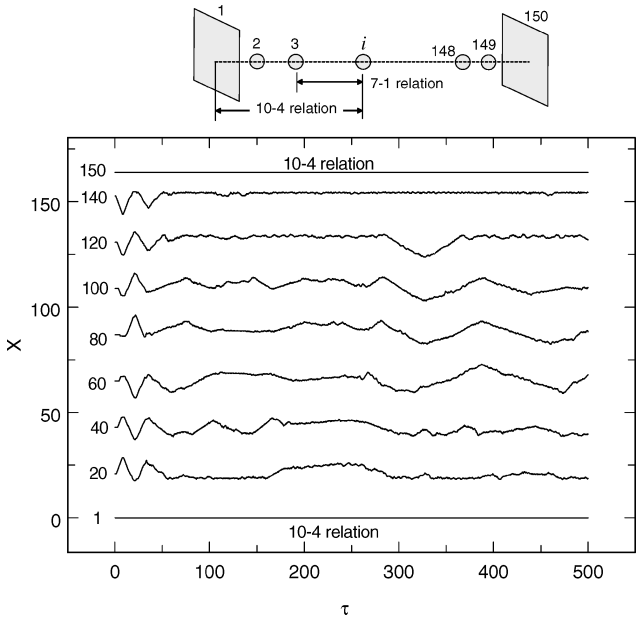

Fig. 10 Dynamic simulation of 148 molecules ($i = 2$ to 149) bounded by two stationary microsurfaces ($i = 1$ and 150). The ratios $M_0/M = 0.1$, $E/E_0 = 0.93$, and $d_0/d = 1.11$. $X_i(0) = 1.1(i-1)$ and $\dot{X}_i(0) = 0$ for $i = 1, \ldots, 150$; $\dot{X}_1(\tau) = 0, \dot{X}_{150}(\tau) = 0$.

agreement shown in Fig. 9, however, the case of $N = 150$ shall be used herewith. This should be sufficient in view of the fundamental characteristics of cluster potential targeted in this work. In Fig. 9, for $N = 150$, the averaged temperature is $\bar{\theta} = 1.7 \times 10^{-4}$, and the peak value of the probability occurs at $\bar{V} = 0$. The system parameter such as the molecular density m and the cluster mass M once again, will not affect the nondimensional results shown in Fig. 9. The multiplying factor in converting the nondimensional velocity V to that in the physical space $\dot{x}$ on the horizontal axis, however, is proportional to $\sqrt{M/m}$.

One of the unique features in the cluster approach is to describe physical boundaries as clusters of different geometries. Figure 10 shows the dynamic simulation for an assembly consisting of 148 molecules bounded by two stationary surfaces ($i = 1$ and 150). Equation (22) is used as the interaction potential between any molecule ($i = 2$ to 149) and the surface ($i = 1$ or 150), whereas the LJ potential is used between any pair of molecules. Equation (29) for $\bar{F}(D)$ with $\alpha = 1$, $\beta = 1$, $\xi = 12$, and $\eta = 6$, in correspondence with the LJ potential, replaces $\bar{F}_{ij}$ in Eq. (30) for all molecules ($i = 2$ to 149), and the equations of motion involving any planar cluster ($i = 1$ or 150) are modified to include the ratios of mass M_0/M and potential well depth E/E_0:

$$\ddot{X}_j = -\xi\eta\left(\frac{M_0}{M}\right)\left(\frac{E}{E_0}\right)\sum_{\substack{i=1\\ i\neq j}}^{N}\left[\frac{1}{(d_0/d)^{\xi}|X_i - X_j|^{\xi+1}} - \frac{1}{(d_0/d)^{\eta}|X_i - X_j|^{\eta+1}}\right] \tag{35}$$

with $\xi = 10$, $\eta = 4$ (plannar clusters for $i = 1$ or N). Subscript 0 refers to the quantities for molecules. The motion is set forth under the same initial conditions shown in Eq. (32), that is, $X_i(0) = 1.1(i-1)$ and $\dot{X}_i(0) = 0$ for $i = 1, 2, \ldots, 150$; $\dot{X}_1(\tau) = 0$, $\dot{X}_{150}(\tau) = 0$. The ratios are chosen to be $M_0/M = 0.1$, $E/E_0 = 0.93$, and $d_0/d = 1.11$, which are estimated from the potential curves shown in Fig. 5. The molecular motion stabilizes beyond $\tau \cong 50$, with local fluctuations prevailed on the overall stabilizing envelopes. The use of clusters thus eliminates the complicated boundary modeling employed in the MD simulation, which involves no more than a simple change of the repulsive and attractive indices, from $\xi = 12$ and $\eta = 6$ for molecules to $\xi = 10$ and $\eta = 4$ for surfaces, in the present example.

Kinetic Boundary Conditions

As a first-order approximation that neglects the vibrational and rotational energy, the energy absorbed in a cluster array is converted into the kinetic energy in support of translational motion of the clusters. Because the kinetic energy is proportional to the velocity squared, this type of problem can involve the velocity-specified condition. An example is given by

$$V_i(X_i, \tau) = V_0 \exp(-aX_i) \times \exp(-b\tau^2) \quad \text{for} \quad 1 = 1, 2, \ldots, N \tag{36}$$

which resembles the energy absorption rate in metals, with X measured from the heated surface.[18–22] With the first cluster aligned at the origin ($X_1 = 0$), V_0 is the initial velocity of the first cluster calculated from the energy balance:

$$\tfrac{1}{2}Mv^2 = (1-R)J \Rightarrow V_0^2 = 12(1-R)(J/E_0) \tag{37}$$

In Eqs. (36) and (37), parameters a and b characterize the autocorrelation function of the irradiating energy intensity, R represents the reflectivity of the cluster surface, and J represents the incoming energy measured in Joules, which is normalized with respect to the well depth of the spherical-cluster potential E_0.

Heat flux Q and stress Σ in the cluster array can be calculated from Eq. (31) without attributing to any constitutive relation. For an array consisting of 150 spherical clusters, assuming the parametric values for $a = 1$, $b = 1$, and $V_0 = 0.001$, Fig. 11 displays three snapshots of time-averaged temperature, heat flux, and stress (pressure) as $\tau = 500$, 1000, and 1500. No constraint is imposed on the first ($i = 1$) and last ($i = 150$) clusters in the cluster array, which allows energy seepage through the boundaries by other mechanisms, such as thermal radiation. Direct energy conversion produces high temperatures in the frontal portion, $X < 100$ approximately, as shown in Fig. 11a. Temperature in this area oscillates with time caused by rapid collisions among clusters. With the kinetic (absorbed) energy decaying exponentially in both space and time, the temperature level in the cluster array increases from $\tau = 500$ to 1000 and then decreases from $\tau = 1000$ to 1500. This is a clear behavior of thermal waves rather than diffusion. The flat region in $X > 400$, as $\tau = 1500$ and beyond, shows that the temperature is almost uniform across the array, which is a common feature in thin-film heating of lattices by ultrashort pulsed laser.[15–17] A similar behavior is observed in heat flux, top right in Fig. 11b. Except for the frontal portion with $X < 100$, heat flux approaches its equilibrium value ($Q = 0$) for $\tau > 1500$. Measuring the load-bearing capacity of the cluster array, pressure Σ seems to stabilize faster than heat flux and temperature, as shown in Fig. 11c. Local oscillations of pressure remain as time

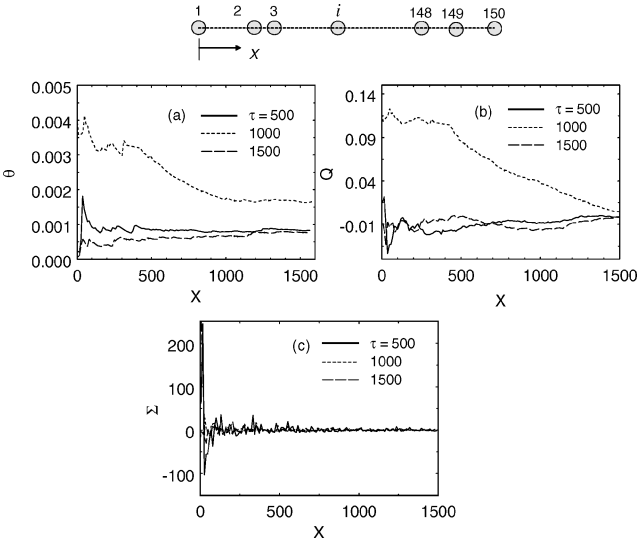

Fig. 11 Dynamic simulation of 150 clusters: a) averaged temperature distribution, b) averaged heat-flux distribution, and c) averaged stress distribution.

increases from 500 to 1500, but the oscillations are confined within a narrower threshold. Compression ($\Sigma < 0$) prevails in the entire domain of the cluster array, reducing in magnitude from $\Sigma \cong -100$ in the front to $\Sigma \cong 0$ in the back. This is a special behavior confirmed by an alternate approach employing the hot-electron blast model.[19,20]

Conclusions

Cluster potentials have been derived in this work. It employs the intermolecular Lennard–Jones (LJ) potential as the Green's function, integrating over various physical domains to yield interaction potentials between clusters of various shapes. The cluster approach is particularly useful for nanoscale assemblies where molecules already congregate in different shapes in forming the building blocks. In addition to clusters of different shapes, the resulting cluster-dynamics (CD) simulation allows for coexistence of molecules in areas where individual molecules remain active, which is a key to multiscale modeling that is essential for microsystems with great complexities.

Asymptotic forms of the cluster potential reveals the fundamental characteristics of CD simulation. Depending on the cluster geometry, the exponents characterizing attractions and repulsions sensitively vary from the 12–6 relation (LJ potential) to the 10–4 relation (molecule to surface), the 9–3 relation (molecule to sphere), the 8–2 relation (surface to sphere), and the 7–1 relation (sphere to sphere). Depicted by the LJ potential that is the source (Green's) function for all of these capricious relations, the difference between the attractive and repulsive exponents is always six. The full expressions for the cluster potential are most useful is studying the dynamic response for both loosely and tightly packed nanoscale assemblies. Radius of the cluster, and consequently the interaction force, enters the CD formulation along with the separation distance. The asymptotic (two-term) approximation can be used for clusters with a characteristic dimension larger than the equilibrium distance for 100 times and beyond.

Because cluster potentials originated from the molecular (LJ) potential, implementation of the cluster model can be readily made in any code for MD simulation. This is particularly true in the use of the asymptotic potentials because the changes often involve no more than the attractive and repulsive components in the code. With compatibilities between CD and MD thus preserved, multiscale modeling involving interactions between molecules and clusters of different shapes can be done almost effortlessly. We have now implemented the cluster model in describing the physical onsets of laser ablation and superheating, by using molecules in critical areas for a better resolution of fast changes and clusters in less sensitive areas. To reveal the refined details, of course, the number of molecules/clusters used in the CD simulation is much larger than that used in the present work.

Rotational and vibrational degrees of freedom can store energy in the clusters, which has been assumed rigid in this work. As the internal energy resulting from these two modes becomes comparable to the translational energy accounted for in the present model, the cluster will no longer be rigid, and additional efforts will be needed to model the interactions among the three types of energy transfer. The distance d in the cluster potential measures the distance between the surfaces of two clusters, which is positive definite. The present treatment does not allow overlapping between two clusters, as the repulsive force will become extremely large at a small value of d that expels the two clusters. The cluster concept does not apply, and the classical molecular dynamics approach needs to be retrieved, when the molecular distribution in the cluster is not dense enough to prevent the overlapping.

The LJ potential is used as a simplest possible example for illustrating the concept of molecular clusters in this work, even though the LJ potential should reveal fundamental phenomena not only for argon but for a wide variety of materials.[22] Semiconductors such as silicon, however, can involve much more complicated internal degrees of freedom than the two-body interaction embedded in the LJ potential. Employing the three-body (SW) potential for silicon, we have been deriving the cluster potential in terms of the base functions involved.

References

[1]Lukes, J. R., Li, D. Y., Liang, X.-G., and Tien, C. L., "Molecular Dynamics Study of Solid Thin-Film Thermal Conductivity," *Journal of Heat Transfer*, Vol. 122, 2000, pp. 536–543.

[2]Wang, X., and Xu, X., "Molecular Dynamics Simulation of Heat Transfer and Phase Change During Laser Material Interaction," *Journal of Heat Transfer*, Vol. 124, 2002, pp. 265–274.

[3]Xu, Y. S., Xiong, D. X., and Tzou, D. Y., "One Dimensional Molecular Dynamics Simulation," *ICHMT Symposium on Molecular and Microscale Heat Transfer in Materials Processing and Other Applications*, Vol. 1, International Centre for Heat and Mass Transfer, Yokohama, Japan, 1996, pp. 49–56.

[4]*ICHMT Symposium on Molecular and Microscale Heat Transfer in Materials Processing and Other Applications*, Vols. 1 and 2, International Centre for Heat and Mass Transfer, Yokohama, Japan, 1996.

[5]Chou, F. C., Lukes, J. R., Liang, X.-G., Takahashi, K., and Tien, C. L., "Molecular Dynamics In Microscale Thermophysical Engineering," *Annual Review of Heat Transfer*, edited by C. L. Tien, Begell House, New York, 1999, pp. 141–176.

[6]Stillinger, F. H., and Weber, T. A., "Computer Simulation of Local Order in Condensed Phases of Silicon," *Physical Review B*, Vol. 31, 1985, pp. 5262–5271.

[7]Tersoff, J., "New Model for the Structure Properties of Silicon," *Physical Review Letters*, Vol. 56, 1986, pp. 632–635.

[8]Car, R., and Parrinello, M., "Unified Approach for MD and Density Functional Theory," *Physical Review Letters*, Vol. 55, 1985, pp. 2471–2474.

[9]Debernardi, A., Bernasconi, M., Cardona, M., and Parrinello, M., "Infrared Absorption in Amorphous Silicon from Ab Initio Molecular Dynamics," *Applied Physics Letters*, Vol. 71, 1997, pp. 2692–2694.

[10]Foiles, S. M., "Application of the Embedded-Atom Method to Liquid Transition Metals," *Physical Review B*, Vol. 32, pp. 3409–3415.

[11]Kotake, S., *Molecular Thermo-Fluid Dynamics*, Maruzen, Japan, 1992.

[12]Iwaki, T., "Molecular Dynamics Study of Stress-Strain in Very Thin Film (Size and Location of Region Defining Stress and Strain)," *Japanese Society of Mechanical Engineers*, Vol. 61A, 1995, pp. 319–327.

[13]Siegel, R. W., "Creating Nanophase Materials," *Scientific American*, Dec. 1996, pp. 74–79.

[14]Tzou, D. Y., Chen, J. K., Roybal, R., and Beraun, J. E., "Cluster Dynamics for Multiscale Interactions," American Society of Mechanical Engineers, July 2003.

[15]Choi, S. U. S., "Enhancing Thermal Conductivity of Fluids with Nanoparticles," *Developments and Applications of Non-Newtonian Flows*, edited by D. A. Siginer and H. P. Wang, FED–Vol. 231/MD-Vol. 66, The American Society of Mechanical Engineers, New York, 1995, pp. 99–105.

[16]Choi, S. U. S., Zhang, Z. G., Yu, W., Lockwood, F. E., and Grulke, E. A., "Anomalous Thermal Conductivity Enhancement in Nano-Tube Suspensions," *Applied Physics Letters*, Vol. 79, 2001, pp. 2252–2254.

[17]Abramson, A. R., Tien, C. L., and Majumdar, A., "Interface and Strain Effects on the Thermal Conductivity of Heterostructures: A Molecular Dynamics Study," *Journal of Heat Transfer*, Vol. 124, pp. 963–970.

[18]Qiu, T. Q., and Tien, C. L., "Short-Pulse Laser Heating on Metals," *International Journal of Heat and Mass Transfer*, Vol. 35, 1992, pp. 719–726.

[19]Qiu, T. Q., Juhasz, T., Suarez, C., Bron, W. E., and Tien, C. L., "Femtosecond Laser Heating of Multi-Layered Metals—II. Experiments," *International Journal of Heat and Mass Transfer*, Vol. 37, 1994, pp. 2799–2808.

[20]Tzou, D. Y., Chen, J. K., and Beraun, J. E., "Ultrafast Deformation in Femtosecond Laser Heating," *Journal of Heat Transfer*, Vol. 124, 2002, pp. 284–292.

[21]Tzou, D. Y., Chen, J. K., and Beraun, J. E., "Hot-Electron Blast Induced by Ultrashort-Pulsed Lasers in Layered Media," *International Journal of Heat and Mass Transfer*, Vol. 45, 2002, pp. 3369–3382.

[22]Kristensen, W. D., Jensen, E. J., and Cotterill, R. M. J., "Thermodynamics of Small Clusters of Atoms: A Molecular Dynamics Simulation," *Journal of Chemical Physics*, Vol. 60, pp. 4161–4169.